NORTHERN ILLINOIS UNIVERSITY

JULY, 2011

EVALUATION OF AN INTEGRATED READ-OUT LAYER PROTOTYPE

BY

FAYEZ ABU-AJAMIEH

A THESIS SUBMITTED TO THE GRADUATE SCHOOL IN PARTIAL FULFILLMENT OF THE REQUIREMENTS FOR THE DEGREE MASTER OF SCIENCE

DEPARTMENT OF PHYSICS

Thesis Director:

Gerald C. Blazey

ABSTRACT

EVALUATION OF AN INTEGRATED READ-OUT LAYER PROTOTYPE

Fayez Abu-Ajamieh, Masters

Department of Physics

Northern Illinois University, 2011

This thesis presents evaluation results of an Integrated Read-out Layer (IRL), a proposed concept in scintillator-based calorimetry intended to meet the exceptional calorimetric requirements of the envisaged International Linear Collider (ILC). This study presents a full characterization of the prototype IRL, including exploration of relevant parameters, calibration performance, and the uniformity of response. The study represents proof of the IRL concept. Finally, proposed design enhancements are presented.

ACKNOWLEDGEMENT

I would like to thank Professor Gerald Blazey, the director of my thesis for his valuable guidance. I would also like to thank Vishnu Zutshi, the supervising scientist of the NICADD detector research group for his constant assistance and follow-up. I would also like to thank the Electrical Engineering Department at Fermilab, especially Paul Rubinov and Tom Fitzpatrick for assembling the IRL board and for their crucial technical assistance, in addition to Christian Gingu for his assistance with the firmware. I would also like to thank Sasha Dychkant for his assistance, and Philip Stone of NIU's Physics Department Machine Shop for manufacturing the jig.

TABLE OF CONTENTS

List of Tables

List of Figures

Figure Page

CHAPTER ONE

CALORIMETRY AND NEW PHYSICS

The search for new physics beyond the Standard Model has gained increased importance over the past years in High Energy Physics (HEP). The search for the Higgs boson, Super Symmetry (SUSY) and extra dimensions are among a few of the main objectives of particle physicists today.

The Large Hadron Collider (LHC) at the European Center for Nuclear Research (CERN) in Geneva, Switzerland, is currently the prime tool physicists use to search for new physics. The LHC is a proton-proton synchrotron collider 27 km in circumference, with a maximum center-of-mass energy of 14 TeV [1]. Since protons are made of quarks and are not elementary [2], measurements at the LHC have only fair accuracy and resolution.

The envisaged International Linear Collider (ILC) is intended to supplement the LHC. The intended center-of-mass energy of the ILC is 500 GeV, with a possible upgrade to 1 TeV [3]. The ILC employs electrons and positrons as accelerated particles. The fact that electrons and positrons are point-like elementary particles leads to better resolution and cleaner events.

The working environment of the ILC will be characterized by small cross sections (of order of 0.1 fb), high luminosity, and high multiplicity final states (6 – 8 jets) [4]. To effectively capture the physics with such low cross sections requires jet energy resolution of order $30\% / \sqrt{E/GeV}$ [5].

The detectors will enclose the collision points of the ILC and record every collision and every scattering product. To ensure recording of all collision information, millions of readout channels are needed for the detectors [6]. Therefore, exceptional calorimetry capabilities that provide precision measurements in a multi-jet environment lie at the heart of realizing the objectives of the ILC. Furthermore, the high number of channels needed for the ILC causes serious installation and integration challenges.

To achieve the required calorimetric capabilities, and to overcome problems related to the integration of millions of channels, the Northern Illinois Center for Accelerator and Detector Development (NICADD) has proposed a new concept called the Integrated Read-out Layer (IRL) for hadron calorimetry. The IRL incorporates the concepts of scintillator-based calorimetry with the proven detection technology of Multi-Pixel Photon Counters (MPPC's) [7]. The IRL is a board on which MPPC's and other electronics are installed. High-granularity scintillator is directly coupled to it (that is without using optical fibers), and the whole system is connected to front-end electronics [7].

The high sensitivity of MPPC's to light, coupled with their insensitivity to magnetic fields, makes them ideal for operating in the ILC environment and allows for excellent resolution; since their signals can be clearly discriminated. The direct coupling of the IRL eliminates the need for optical fibers for transmitting light to the MPPC's, which makes integration of the ILC's myriad channels relatively simple.

In this thesis, an in-depth characterization of the prototype IRL is presented, followed by the suggested enhancements and the prospects for future use.

CHAPTER TWO

THE IRL DESIGN AND TESTING APPARATUS

The IRL board is made of several electronic components that serve a variety of functions; including control, signal processing and amplification, input/output functionalities and biasing. Surface mounted Light Emitting Diodes (LEDs) are installed on specific locations on the board, with MPPCs surrounding each. An array of high granularity scintillating cells is directly coupled to the board, covering the LEDs and MPPCs. The IRL board is connected to front-end electronics that control the input signals and process the output signals.

2.1. MPPC

The MPPC, also known as a Silicon Photomultiplier (SiPM), is a photon counting device consisting of multiple Avalanche Photodiode (APD) pixels operating in the limited Geiger mode [8]. Hamamatsu SiPM's (see Figure 2.1) of 25, 50 and 100 micron pixels were used as sensors in the IRL.

Detectors in the ILC might be placed in a high radiation region, which might damage electronics or give rise to unwanted signals. Therefore, detectors to be used in the ILC should be designed to properly operate under condition of high radiation. The main advantages of SiPM's include their high sensitivity (depending on the number of pixels), small size, low operational voltage, and their insensitivity to magnetic fields, which make them ideal for the ILC purposes. In addition, in large quantities they should be

inexpensive, which will contribute to the cost-effectiveness of the detector. The main drawback of SiPM's, however, is their sensitivity to temperature changes.

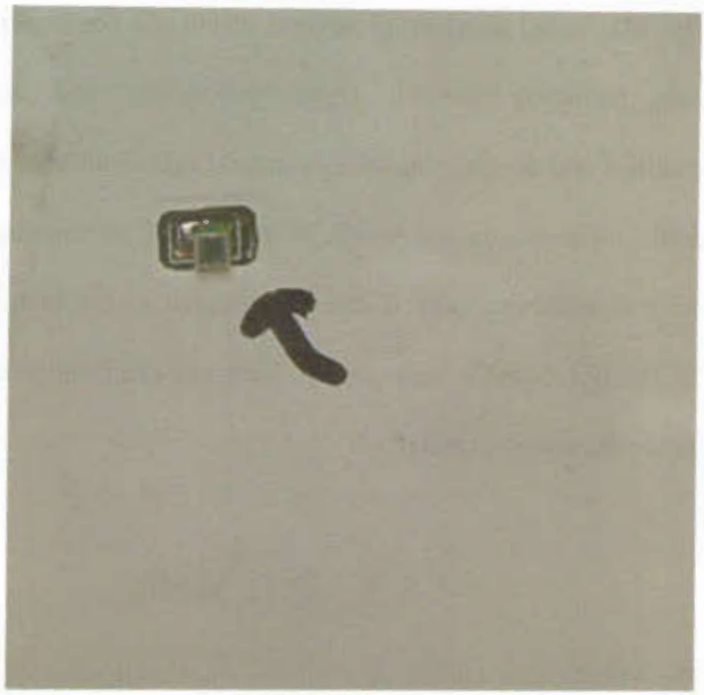

Figure 2.1: Hamamatsu SiPM mounted on the IRL board: The sensitive surface can be seen. (Size of the SiPM is 1mm X 1mm)

2.2. Scintillator and Dimpled Cells

Scintillator is a material that converts ionization energy loss into light. When radiation or high energy particles interact with the material of the scintillator, molecules are excited to higher energy levels. When an excited molecule returns to its ground state, it can emit a photon. This phenomenon is known as radioluminescence or scintillation [9]. Scintillators can be either organic or inorganic. Often dyes are used to absorb and re-

emit the radiation at different wavelengths; these are called wavelength shifting scintillators.

The scintillating material used for the IRL was fabricated in an array of 5 X 5 square dimpled cells as shown in Figure 2.2. Each cell is 9 cm^2 in area and 5 mm in thickness. The dimple or concavity is 3 mm deep. A mirror film of VM2000 covers the flat face of the scintillator in order to efficiently reflect light. The sides of the cells are painted with white EJ510. The cell is directly coupled to an SiPM mounted on the IRL board as shown in Figure 2.3. Part of the light generated by the cell is captured by the SiPM, which converts it to an electrical signal that can be measured and calibrated [7].

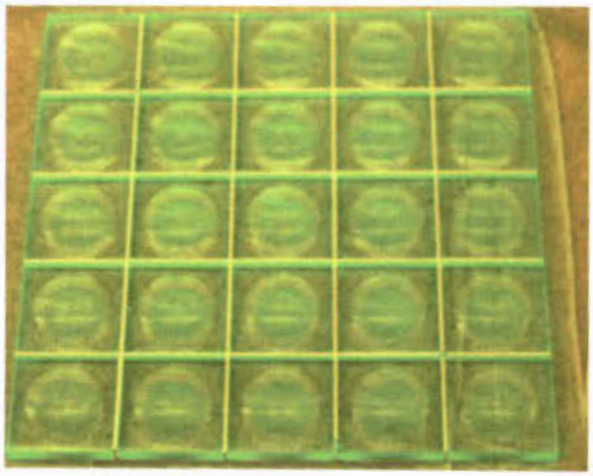

Figure 2.2: A 5 X 5 scintillator grid made of square dimpled cells. The tiles are separated by white paint.

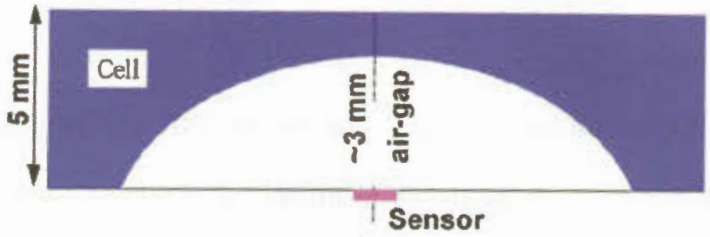

Figure 2.3: Cell mounting on the SiPM: The concave cell is flush with the SiPM, with the air gap directly above it.

The main advantage of the dimpled cells lies in their uniform response which is independent of the particle impact position [7]. Figure 2.4 shows the response of a 9 cm^2 square dimpled cell as a function of the position of a radioactive source.

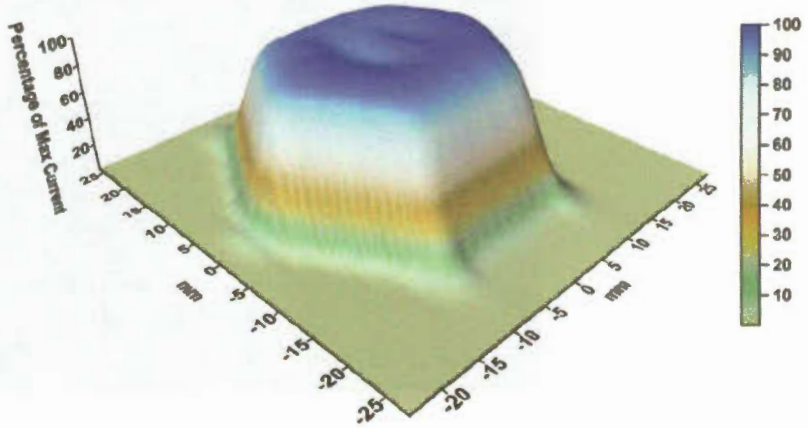

Figure 2.4: Cell response uniformity as a function of source position.

2.3. IRL Board

The IRL board is a Printed Circuit Board (PCB) on which the SiPMs are mounted, and to which the scintillator is directly coupled. The IRL provides the bias required for the SiPMs and carries the signals to the front-end electronics [7]. Up to 64 SiPMs can be

installed on one IRL board. A reflective layer is printed on the board to maximize the amount of light captured by SiPMs and to ensure that the scintillator is flush with the sensitive surface of SiPMs. The main components of the IRL are (see Figure 2.5):

- Field-Programmable Gate Array (FPGA): A programmable integrated circuit that holds the control logic for the IRL board.
- Application Specific Integrated Circuits (ASIC's): Several chips that provide signal processing and amplification.
- Low Voltage Differential Signaling (LVDS) transceiver and connector: The communication protocol between the IRL board and the front-end electronics.
- Bias Generator: Provides bias voltage for the SiPMs.
- Calibration Ultraviolet Light Emitting Diodes (UV LEDs), together with their supporting circuitry, provide a calibration light source for the SiPMs.

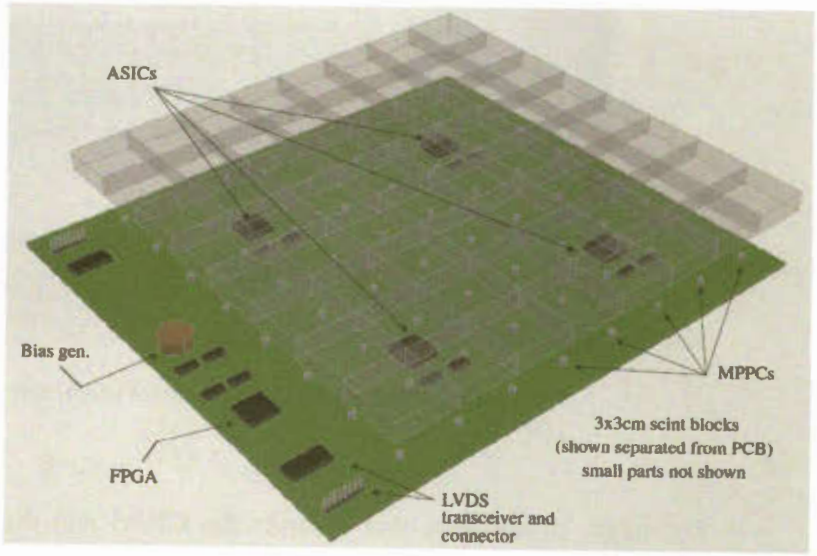

Figure 2.5: IRL board design and main components.

2.4. Testing Environment and Front-End Electronics

For the purposes of testing, UV LEDs were used as a light source for calibration. To ensure that no other light source could contaminate the signals of the SiPMs, the board was placed in a light-tight black box.

The IRL board was connected to a Chain Read-out Connector board (CROC), which is in turn was connected to a Chain Read-out Interface Module (CRIM). These front-end electronic boards are custom-made by the Electrical Engineering Department at Fermilab for board-testing purposes [10]. They control the IRL board and received the SiPMs signals. Figure 2.6 shows these front-end electronics.

Figure 2.6: Front-end electronics: CRIM (right) and CROC (left).

By means of software that controls the CRIM and the CROC, the various IRL testing parameters, such as the LED input pulse width and amplitude, delays and MPPC

bias voltage are manipulated. Root 5.20/00 was used to analyze output data and generate histograms. The histograms provide the mean and RMS of the SiPM's response to an input light pulse.

CHAPTER THREE

PRELIMINARY CHARACTERIZATION

Prior to embarking on characterizing the board, it was important to reach a general understanding of IRL board operation and the impact of manipulating the various parameters (such as the pulse width and amplitude) on the output. Therefore, data runs were taken using a 25-micron-pixel SiPM mounted on the IRL board with an external LED as a light source. The results were used as the starting point for subsequent analyses.

3.1. Gate Start Determination

The Gate Start refers to the time delay separating the beginning of the data run and the instant at which the CROC begins integrating the signal. The Gate Length represents the time interval over which SiPM signals are integrated. The Gate Start is the relative time at which the gate is opened to integrate the signal and is determined through the software with possible values ranging from 0 to 65500 ticks, where a tick refers to the crystal oscillation of the FPGA. The time interval of one tick is 9.4 ns. The LED Delay is the time after the Gate Start at which the LED receives current. Figure 3.1 shows a schematic of the Gate Start, Gate Length, and LED Delay.

In order to determine the Gate Start, an external LED was used to flash light on a 25-micron-pixel SiPM mounted on the IRL board. A pulse generator was used to deliver an electric pulse to the LED, and the gate control parameter was scanned from 65000 to 65500. The Gate Length was set at 13 ticks (~122 ns), and measurements at each Gate Start value were taken twice: once with the LED turned on and the other with it turned

off. The mean values of the histograms generated by Root were plotted against the Gate Start parameter as shown in Figure 3.2. The case with the LED off gives rise to a flat response corresponding to pedestal (integrated noise), while the latter case gives rise to a detectable response that peaks at a value of 65446, which is chosen as the nominal Gate Start.

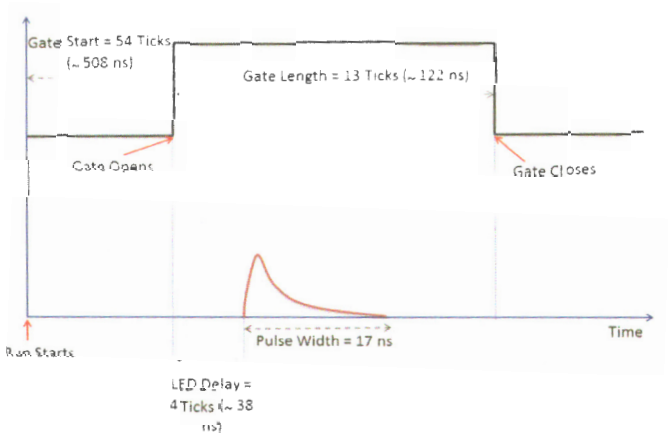

Figure 3.1: Schematic of Gate Start and the relevant delays (not to scale)

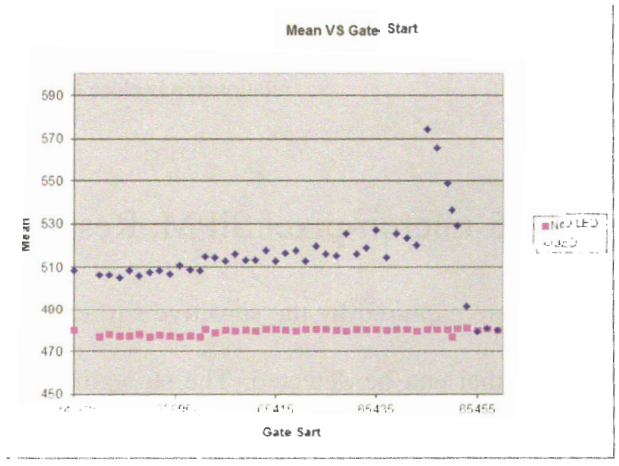

Figure 3.2: Histogram mean as a function of Gate Start delay:

The peak resides at the optimal value to start the gate.

3.2. Pulse Amplitude Effect

Increasing the pulse amplitude increases the amount of light emitted by the LED. Therefore, the SiPM's response mean is expected to have some dependence on the amplitude. This dependence turned out to be almost linear as shown in Figure 3.3. The mean and RMS values are automatically calculated by Root when generating the histograms.

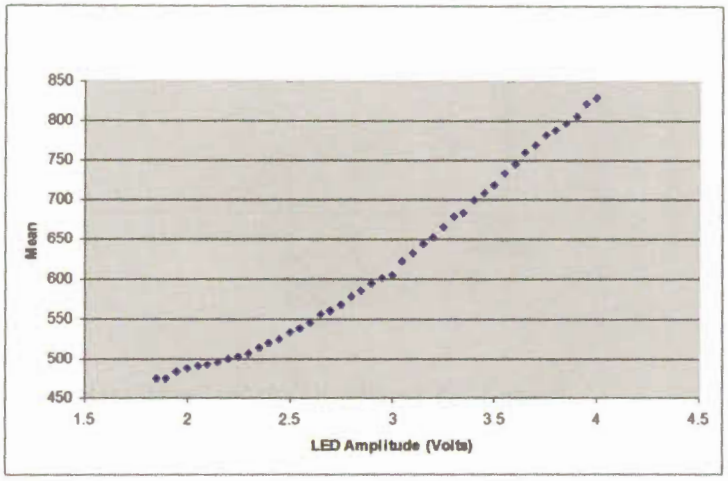

Figure 3.3: SiPM's response as a function of LED amplitude: The relationship is close to linear.

3.3. 25-micron-pixel SiPM: Response and Saturation

As photons are captured by the sensitive surface of the SiPM, each APD generates an electric signal that can be detected. The strength of the signal is proportional to the number of photons detected, which appear as peaks in a response histogram. Such peaks are called photoelectron peaks.

A 25-micron-pixel SiPM was installed on the IRL board and an external LED was used to deliver a light pulse. The 25-micron-pixel SiPM is indeed capable of detecting the light emitted, as demonstrated by the increase in the values of the response mean and RMS. However, due to its lower gain, no discernible photoelectron peaks can be observed in the histograms, regardless of the amount of light emitted.

As the amount of light is increased; the mean of the SiPM response increases until saturation of the SiPM occurs. Saturation occurs due to limitations in the circuitry; namely the amplification circuit which amplifies the SiPM's response, and the Analogue to Digital Convertor (ADC) which converts the analogue response into digital values. Amplification higher than needed, combined with the fact that the ADC only provides 11-bits (which makes the range available $2^{11} = 2047$ including zero) leads to saturation at that value. At saturation, the distribution is clipped and the response is no longer reliable. Figure 3.4 shows the response of a 25-micron-pixel SiPM to a 2.6 V pulse. The distribution at 2047 ADC counts is clipped due to the onset of saturation.

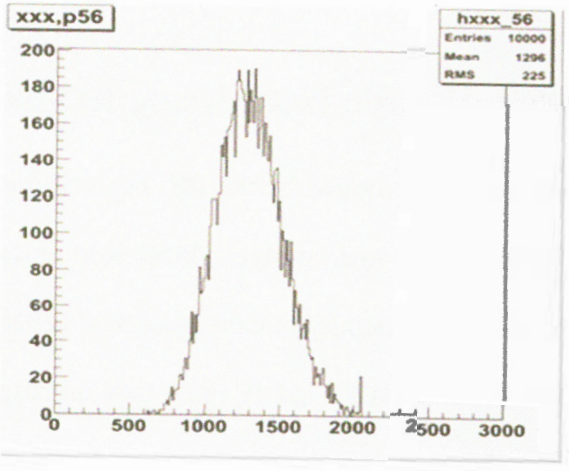

Figure 3.4: Response of a 25-micron-pixel SiPM to a 2.6V pulse: Saturation is observed at 2047 ADC values.

CHAPTER FOUR

IRL PROOF OF CONCEPT

Having understood the basic characteristics and functions of the IRL, it was essential to determine whether or not the board operates according to design objectives, i.e. whether the SiPMs could capture light and show a clean response characterized by photoelectron peaks. This required synchronization of the IRL board with the front-end electronics. In addition, it was necessary to reach an understanding of the proper values of the parameters needed for analysis, such as the amount of light needed to activate the SiPMs and the proper Gate Length.

Throughout this study, 100-micron-pixel and 50-micron-pixel SiPMs were used and compared. Although a 100-micron-pixel SiPM is much more sensitive than a 50-micron-pixel one, the latter has lower gain. This means that for the same amount of light, the mean and RMS will be lower, which means that the issue of saturation is expected to be less severe.

4.1. Photoelectron Peaks Using 100-micron-pixel SiPMs

The sensitivity level required by the IRL board is higher than that of a 25-micron-pixel SiPM. Therefore, 100-micron-pixel SiPMs were installed on the IRL board. These SiPMs were located in the vicinity of calibration UV LEDs, as shown in Figure 4.1. The calibration LEDs are labeled A and B since they are triggered separately through the software. The scintillator is directly coupled to the board such that each SiPM is covered by one tile, while each LED lies at the corner of four tiles.

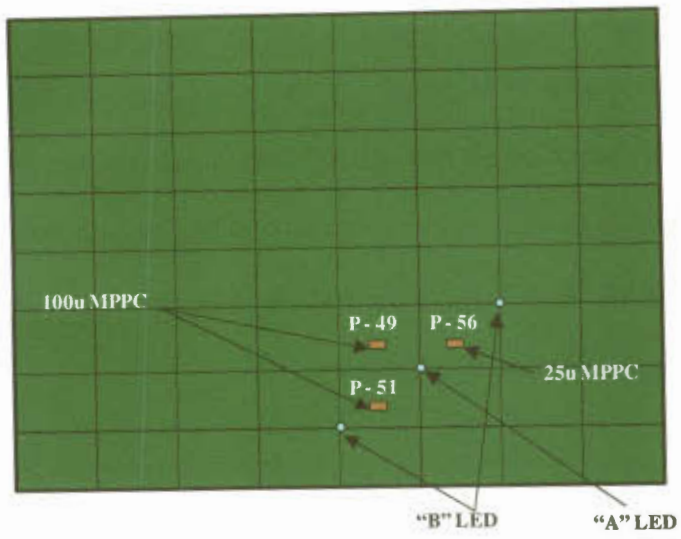

Figure 4.1: SiPMs installation on the IRL board.

4.1.1. Observing Photoelectron Peaks

Due to the saturation limitation of the circuitry providing input to the FPGA (namely the amplification circuit and the Analogue to Digital Convertor (ADC), as discussed in Section 3.3) the amount of light emitted by the LEDs must be optimized. A Pulse Width of 17 ns with amplitude of 2.1 V provided optimal results for 100-micron-pixel SiPMs.

The IRL has two gain channels; a High Gain (HG) channel and a Low Gain (LG) channel. For 100-micron-pixel SiPMs, it was found that the HG channel either shows no response (for small pulse widths) or experiences rapid saturation (i.e. saturation prior to observing photoelectron peaks) for the higher LED pulse widths. Figure 4.2 shows a sample of SiPM responses: The histograms are titled P49, P50, P51, P53, P54 and P59 corresponding to the physical locations of the SiPMs on the IRL board. Only P49 and P51 had SiPMs mounted, while the other locations were empty (those locations are available for installing additional SiPMs). In the right-most panels saturated response of

the SiPMs can be seen for P49 and P51 (upper and lower right-most canvasses); although photoelectron peaks exist, much of the histograms are clipped due to saturation. Therefore the output of the HG channel is excluded. On the other hand, the LG channel exhibits clear peaks with limited or no saturation using a pulse 17 ns in width and 2.1 V in amplitude. Figure 4.3 shows the response with the LG channel for the same SiPMs; saturation is either absent or insignificant.

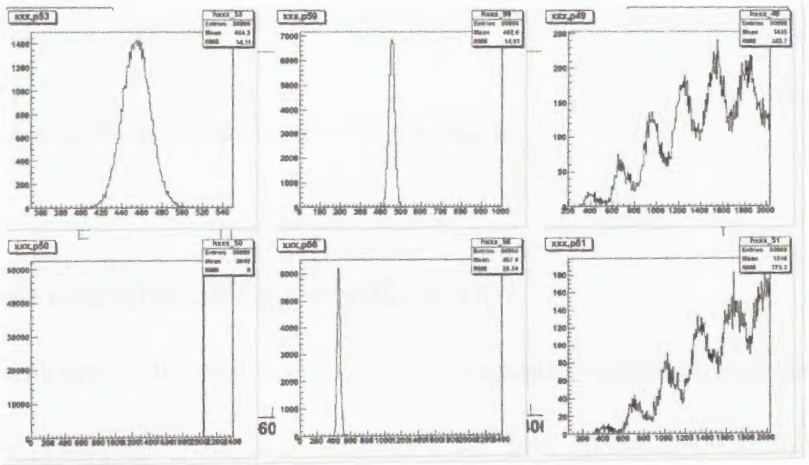

Figure 4.2: Response of the 100-micron-pixel SiPMs on the HG channel.

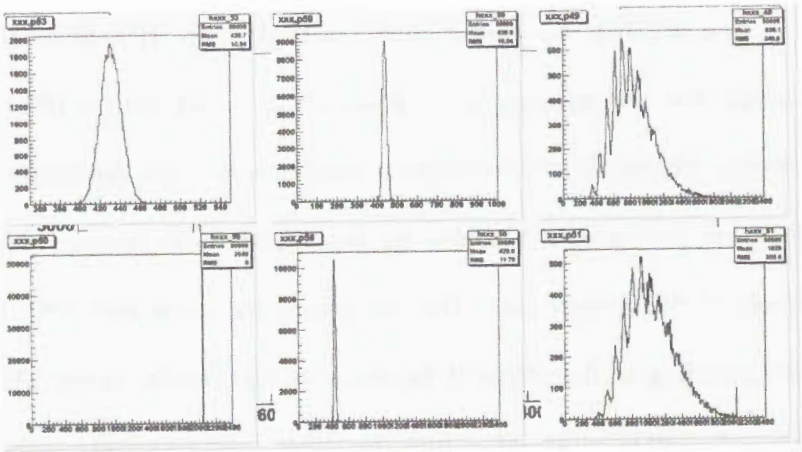

Figure 4.3: Response of the 100-micron-pixel SiPMs on the LG channel.

4.1.2. SiPM Response Mean and RMS

As illustrated in Figure 3.1 above, the LED Delay refers to the time interval between the Gate Start and the beginning of the input pulse delivered to the LEDs. It can also be inferred from the same figure that the only possible ways to manipulate the amount of light detected by the SiPM are the LED pulse amplitude, width and delay. In order to determine how the response changes as a function of the LED Delay, and to determine the delay that yields the best response in terms of peak clarity, data was taken while varying the LED Delay from 0 to 13 ticks. The mean and RMS tend to increase by increasing the LED Delay, reaching a maximum at 4 or 5 ticks before dropping again as shown in Figures 4.4 and 4.5. Photoelectrons peaks are most discernible at these two delay values.

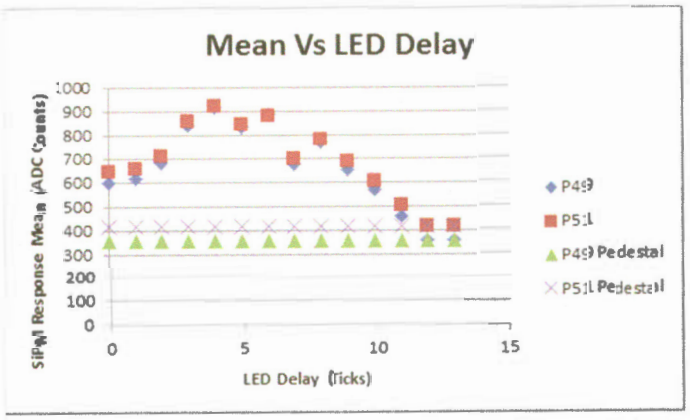

Figure 4.4: The mean of the 100-micron-pixel SiPMs response as a function of LED Delay. The flat curves are pedestal.

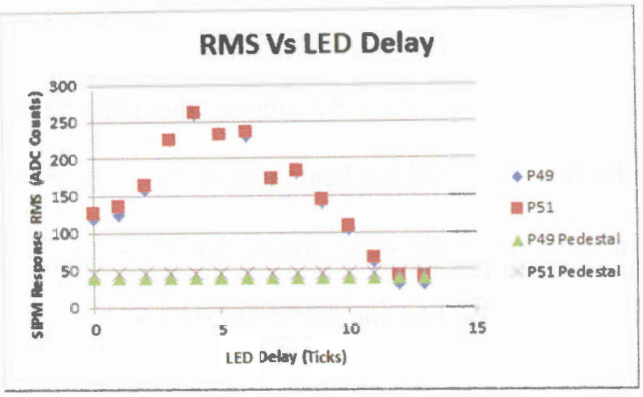

Figure 4.5: The RMS of the 100-micron-pixel SiPM response as a function of LED Delay.

4.1.3. Gain Calculation

Clearly discernible photoelectron peaks were fit with a Gaussian function and their corresponding means were calculated. The average separation of the photoelectron peaks is taken as the gain on the SiPM in units of ADC counts per photoelectron peak. Table 4.1 shows a sample gain calculation.

	P49 (ADC counts)	**P51 (ADC counts)**
Peak 1 - Pedestal	93.3	100.1
Peak 2 – Peak 1	93.4	99.6
Peak 3 – Peak 2	93.1	98.3
Peak 4 – Peak 3	NA	99.3
Gain (Average)	**93.3 ± 0.6**	**99.3 ± 0.5**

Table 4.1: Gain calculation for two 100-micron-pixel SiPMs: P49 and P51 refer to the physical locations of the SiPMs on the IRL board.

4.1.4. Gain and Bias Voltage

SiPMs gain depends on bias voltage. While taking measurements, SiPMs are biased according to the values specified by the manufacturer. Figure 4.6 shows the gain of one 100-micron-pixel SiPM as a function of its bias voltage; the dependence is fit with a line.

This fit can be used to extrapolate the gain values at different bias voltages in order to use them for calculating the light uniformity distribution (to be discussed in the next chapter) should the SiPMs be biased according to bias voltages other than those specified by the manufacturer.

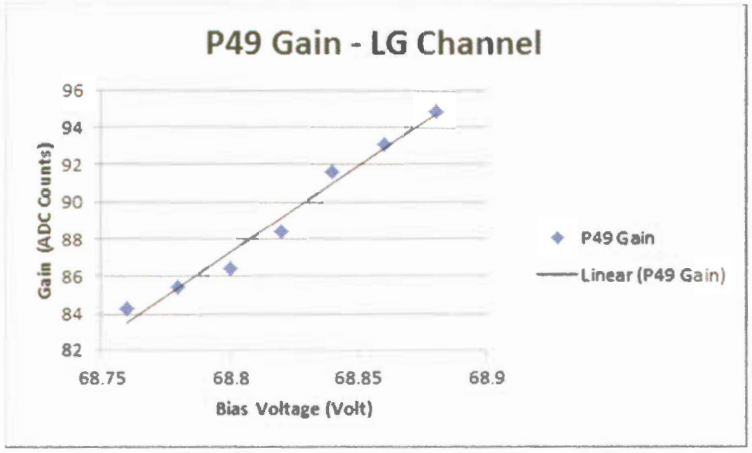

Figure 4.6: The gain of a 100-micron-pixel SiPM (in units of ADC/PE) as a function of bias voltage (in units of volt).

4.2. Photoelectron Peaks Using 50-micron-pixel SiPMs

Similar measurements were taken with 50-micron-pixel SiPMs which experience limited or no saturation at any LED Delay with both the HG and LG channels. However, unlike the 100-micron-pixel ones, they exhibit photoelectron peaks only on the HG

channel. Therefore, only the HG channel was considered for analyzing the response of 50-micron-pixel SiPMs.

4.2.1. Observing Peaks

The 50-micron-pixel SiPMs are less sensitive to light than the 100-micron-pixel ones. Therefore, a 17 ns pulse is not sufficient to produce any response. The only alternative is to use a pulse 19 ns in width and 2.5 V in amplitude. However, the amount of light generated by a 19 ns pulse is too high and leads to early saturation. To control the amount of light received by the SiPM, an optical filter was used. Through this, photoelectron peaks were observed. Figure 4.7 shows the response of four 50-micron-pixel SiPMs to a 19 ns filtered pulse on the HG channel (upper three panels and left-most bottom panel). The four SiPMs were mounted on P49, P51, P53 and P56, whereas the other two locations, namely P59 and P61 were empty. Thus their response simply corresponds to a pedestal.

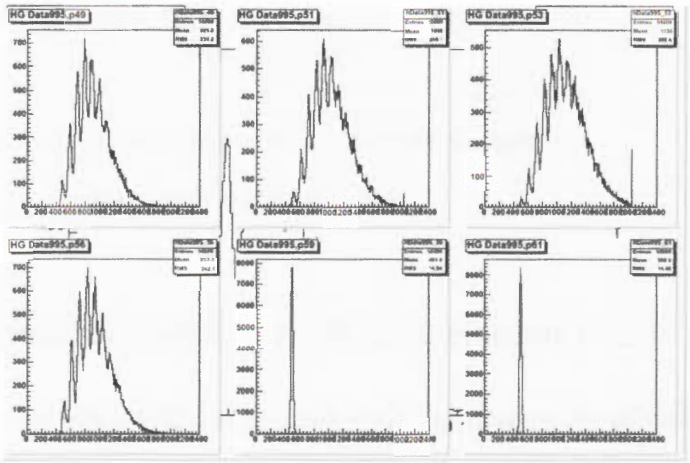

Figure 4.7: The response of four 50-micron-pixel SiPMs to a 19 ns pulse at 3 tick delay. The other lower right locations had no mounted SiPMs.

4.2.2. Average Response and Variation

As sown in Figures 4.8 and 4.9, the mean response and variation of the 50-micron-pixel SiPMs as a function of LED Delay from 0 – 13 ticks is similar to that of 100-micron-pixel SiPMs. However, the most discernible peaks are observed at a 3 tick delay compared to 4 or 5 ticks using 100-micron-pixel SiPMs. Therefore, this delay was used for gain calculation purposes.

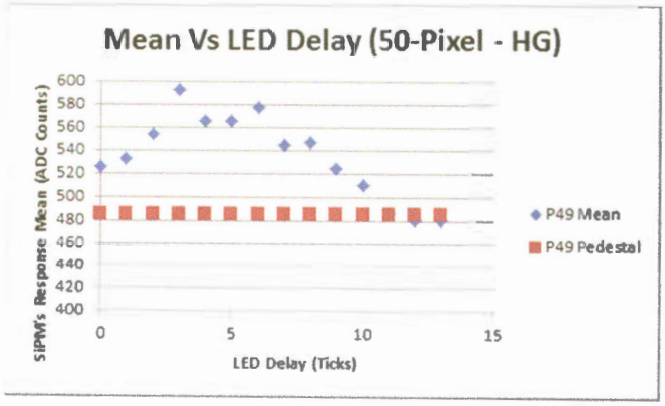

Figure 4.8: The mean of the 50-micron-pixel SiPM response as a function of LED Delay.

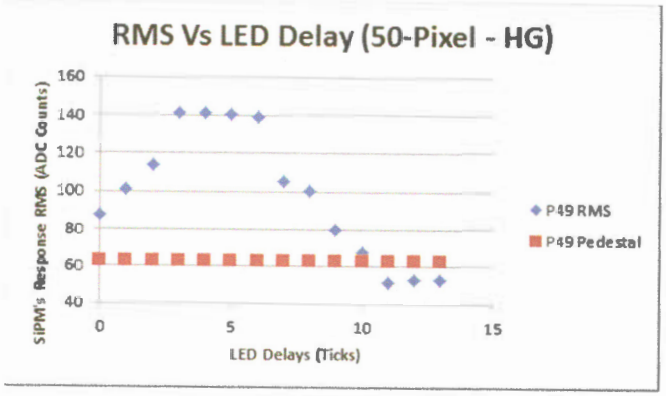

Figure 4.9: The RMS of the 50-micron-pixel SiPM's response as a function of LED Delay.

4.2.3. Gain Calculation

The method described in section 4.1.3 was used to calculate the gain of the 50-micron-pixel SiPMs. As expected, the gain values of the 50-micron-pixel SiPMs are lower than their 100-micron-pixel counterparts. Table 4.2 shows the gain calculation of the four 50-micron-pixel SiPMs.

	P49 (ADC)	**P51 (ADC)**	**P53 (ADC)**	**P56 (ADC)**
Peak 1 - Pedestal	84.9	87.2	83.7	92.8
Peak 2 – Peak 1	89.1	88.4	91.7	89.6
Peak 3 – Peak 2	85.1	89.2	89.3	89.1
Peak 4 – Peak 3	85.9	88	87.7	89.8
Peak 5 – Peak 4	80.2	87.6	87.1	88.4
Gain (Average)	**85.0 ± 0.6**	**88.1 ± 0.7**	**87.9 ± 0.8**	**89.9 ± 0.6**

Table 4.2: Gain calculation for four 50-micron-pixel SiPMs.

4.2.4. Effect of Gate Length

The Gate Length represents the electronic window over which the signal is integrated. The Gate Length is determined in integer multiples of the crystal oscillations of the FPGA. A single oscillation (a tick) has a value of 9.4 ns. Typically, a gate length of 13 ticks (~122 ns) is used.

As the Gate Length is increased with the LED turned off, more noise is available for integration. More integrated noise is expected to cause the RMS to increase. However, the mean should not be affected by this increase in integrated noise.

The situation is different when the LED is on, since the relatively long time constant (τ) of the circuitry leads the LED light pulse to have a relatively long tail that is much longer than the Gate Length as demonstrated by Figure 4.10.

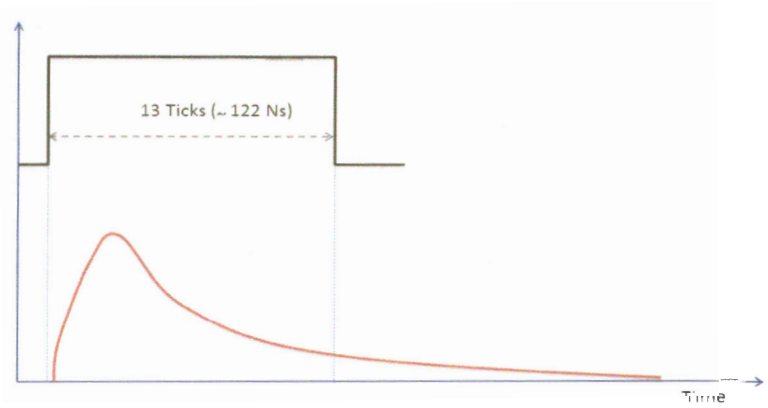

Figure 4.10: Light pulse integration by the electronic gate.

As the Gate Length is increased; the amount of light (which dominates over noise) available for integration becomes higher. The increment in the amount of light as a function of increments in the Gate Length in not constant as a result of the pulse shape and is expected to be decreasing. Furthermore, there should be a value below which the Gate Length is no longer sufficient to capture the signal, or to allow the output of the relevant electronics to reach the required values (as will be discussed later). Therefore, the response should correspond to pedestal values at this point.

Figures 4.11 and 4.12 demonstrate that the behavior described above is indeed correct for both cases (with and without the LED emitting light). The lowest value of the Gate Length were the SiPM's response can be integrated is 6 ticks.

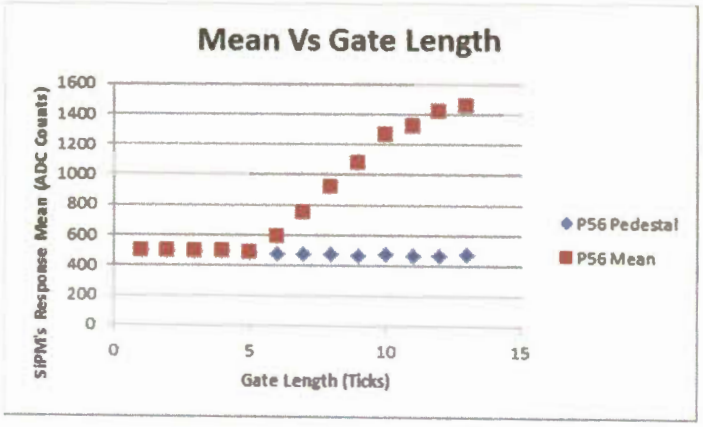

Figure 4.11: SiPM's mean response as a function of the Gate Length.

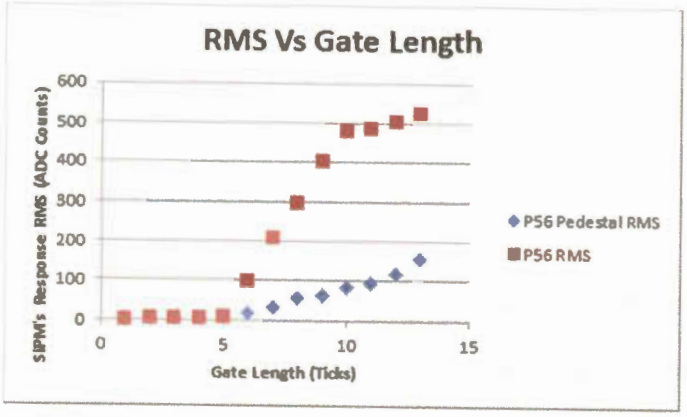

Figure 4.12: SiPM's response RMS as a function of the Gate Length.

4.2.5. Effect of LED Delay

As shown in Figure 4.8 above, the light pulse has a long tail that extends beyond the gate length. This would mean that the LED Delay is expected to affect the SiPMs

response. Figures 4.13 and 4.14 show the responses of a SiPM at 3 and 4 tick delays respectively. The photoelectron peaks are clearer for a 3 tick delay. This is plausible since at this delay, the gate provides more time for integrating light (10 ticks = 94 ns compared to 9 ticks = 84.6 ns for a 4 tick delay). For the purposes of calculating the light distribution uniformity (to be discussed in the next chapter); the delay that yields the clearest results, i.e. 3 ticks for 50-micron-pixel SiPMs and 4 – 5 ticks for 100-micron-pixel SiPMs, was used.

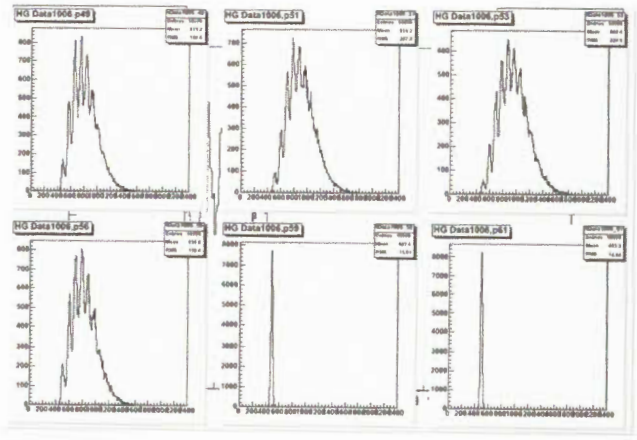

Figure 4.13: 50-micron-pixel SiPM response at a 3 tick LED Delay.

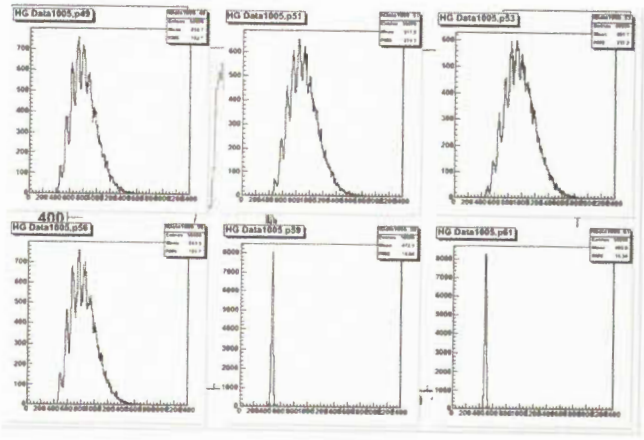

Figure 4.14: 50-micron-pixel SiPM response at a 4 tick LED Delay.

Gain calculation at different LED Delays reveals an ostensible dependence of gain on delay. SiPMs gain, however, should not have any dependence on the amount of light available for integration, since it depends only on the SiPMs and its supporting circuitry. The difference in gain at 3 tick and 4 tick delays was calculated at the same temperature scale in order eliminate the possibility of a temperature related effect. Counter-intuitively, the gain value at a 4 tick delay is roughly 6 – 8% lower than at a 3 tick delay. Figure 4.15 shows a sample comparison between the gain values at both delays, whereas Table 4.3 shows the comparison for the four SiPMs.

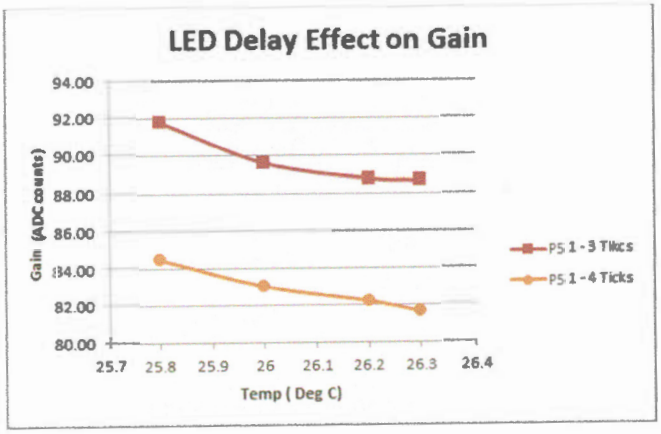

Figure 4.15: Effect of LED Delay on SiPM gain.

Temp (∘C)	P49			P51			P53			P56		
	Delay(ticks)		% Diff.	Delay(ticks)		% Diff.	Delay(ticks)		% Diff.	Delay(ticks)		% Diff.
	3	4		3	4		3	4		3	4	
25.8	90.4 ± 0.2	82.7 ± 0.3	8.50% ± 0.38%	91.8 ± 0.2	84.5 ± 0.3	7.94% ± 0.37%	92.4 ± 0.2	85.2 ± 0.2	7.79% ± 0.32%	94.8 ± 0.2	87.3 ± 0.3	8.00% ± 0.34%
26	87.9 ± 0.2	80.9 ± 0.3	7.91% ± 0.39%	89.6 ± 0.2	83.1 ± 0.3	7.31% ± 0.36%	90.9 ± 0.2	84.3 ± 0.2	7.29% ± 0.31%	92.8 ± 0.2	85.4 ± 0.3	8.07% ± 0.36%
26.2	86.4 ± 0.2	79.6 ± 0.3	7.82% ± 0.46%	88.8 ± 0.2	82.2 ± 0.3	7.38% ± 0.37%	89.3 ± 0.2	82.4 ± 0.2	7.77% ± 0.33%	90.7 ± 0.2	84.0 ± 0.3	7.36% ± 0.38%
26.3	86.7 ± 0.2	79.9 ± 0.3	7.80% ± 0.40%	88.7 ± 0.2	81.6 ± 0.3	7.92% ± 0.37%	89.0 ± 0.2	82.7 ± 0.2	7.08% ± 0.33%	90.4 ± 0.2	84.6 ± 0.3	6.51% ± 0.37%

Table 4.3: LED Delay effect on gain.

To resolve this paradox, gain was calculated with two sets of parameters: The first using a 13 tick Gate Length and a 3 tick LED Delay, while the other using a 14 tick Gate length and a 4 tick LED Delay. If gain does not depend on the LED Delay (as is believed) then the gain values of both cases should be identical save statistical variation. As Table 4.4 below shows, the gain values for both cases are within acceptable statistical variation, which means that gain is independent of LED Delay. The reason for the ostensible dependence lies in the slowness of the integrator. The integrator is a chip that integrates current output from the SiPM. The integrator has a long time constant (30 ns). Therefore, at a certain LED Delay, the integrator has insufficient time to reach its maximum value,

which reduces the overall output of the SiPM, causing its response to appear to have a lower gain.

SiPM	Gain		
	3 Tick Delay (GL = 13 Ticks)	4 Tick Delay (GL = 14 Ticks)	% Difference
P49	90.4 (± 0.2)	90.3 (± 0. 2)	0.07% (± 0.31%)
P51	91.8 (± 0.2)	91.7 (± 0.3)	0.12% (± 0.35%)
P53	92.4 (± 0.2)	93.0 (± 0.2)	0.64% (± 0.32%)
P56	94.8 (± 0.2)	94.4 (± 0.2)	0.43% (± 0.33%)

Table 4.4: Comparison between gain values at 3 tick delay with a 13 tick Gate Length and 4 tick delay with a 14 tick Gate Length.

CHAPTER FIVE

LIGHT DISTRIBUTION UNIFORMITY

Light distribution uniformity refers to the different light levels received by each SiPM placed equidistantly from one calibration LED relative to the average amount of light received by all SiPMs. The SiPMs need to be calibrated in two regimes: the low light and high gain regime, which is used for calibrating the SiPMs gain; and the high light and low gain regime, which is needed to determine operating parameters to avoid saturation. For proper operation of the IRL, both calibration regimes require a uniform distribution of light among the SiPMs.

5.1. Light Distribution Uniformity Using 100-micron-pixel SiPMs

5.1.1. Low Gain Channel

Four 100-micron-pixel SiPMs were installed around one of the calibration UV LEDs as shown in Figure 5.1. An LED pulse of width 17 ns and amplitude 2.1 V in was used. The LG channel was used since it does not lead to SiPMs saturation, and the SiPMs were optimally biased. Data runs were taking while varying the LED Delay from 13 – 0 ticks.

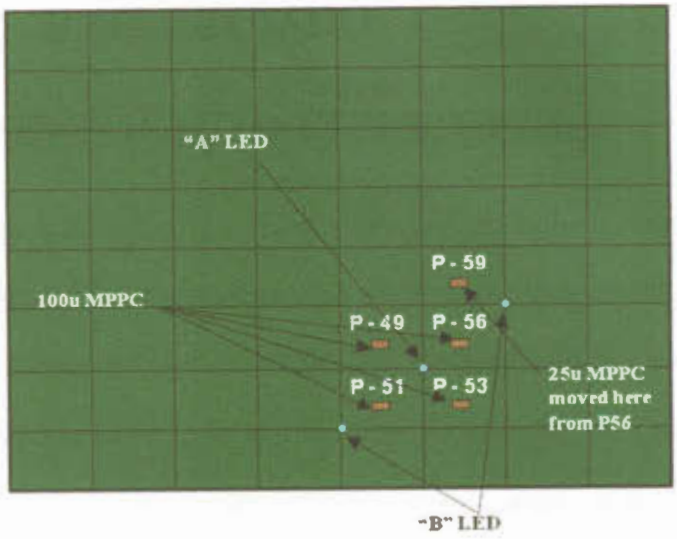

Figure 5.1: SiPMs mounting of the IRL board: Only the A LED was used for calculating the light distribution uniformity.

The light distribution uniformity was calculated for non-saturating delay values using the following formula for the light response:

$$Light\ Response = \frac{Mean\ (ADC) - Pedestal\ (ADC)}{Gain\ (ADC)}$$

Points taken at LED Delays of 11, 12, and 13 were excluded since the amount of light detected was negligible and the response cannot be distinguished from pedestal beyond statistical variations.

The average light response was calculated for every SiPM and then the overall average for all four SiPMs was determined. Finally, the percent deviation of the SiPM individual mean from the overall mean was taken as a measure of the relative excess or deficit of light each SiPM received. Table 5.1 shows a sample calculation of the light distribution uniformity.

LED Delay (Ticks)	P49				P51				P53				P56			
	Mean	Ped.	Gain	Light Response	Mean	Ped.	Gain	Light Response	Mean	Ped.	Gain	Light Response	Mean	Ped.	Gain	Light Response
13	355.0	355.1	39.3	0.0	414.2	414.2	44.6	0.0	424.0	424.1	39.4	0.0	427.4	427.6	42.8	0.0
12	354.0	355.1	39.3	0.0	413.3	414.2	44.6	0.0	422.8	424.1	39.4	0.0	426.3	427.6	42.8	0.0
11	369.6	355.1	39.3	0.4	431.1	414.2	44.6	0.4	435.0	424.1	39.4	0.3	441.2	427.6	42.8	0.3
10	443.6	355.1	39.3	2.3	513.2	414.2	44.6	2.2	494.2	424.1	39.4	1.8	512.3	427.6	42.8	2.0
9	541.8	355.1	39.3	4.7	621.2	414.2	44.6	4.6	573.7	424.1	39.4	3.8	609.2	427.6	42.8	4.2
8	615.9	355.1	39.3	6.6	704.5	414.2	44.6	6.5	632.5	424.1	39.4	5.3	683.2	427.6	42.8	6.0
7	670.4	355.1	39.3	8.0	768.6	414.2	44.6	8.0	677.1	424.1	39.4	6.4	734.5	427.6	42.8	7.2
6	771.1	355.1	39.3	10.6	877.4	414.2	44.6	10.4	755.8	424.1	39.4	8.4	733.3	427.6	42.8	7.1
5	953.5	355.1	39.3	15.2	1082.0	414.2	44.6	15.0	907.2	424.1	39.4	12.2	1011.0	427.6	42.8	13.6
4	794.3	355.1	39.3	11.2	910.5	414.2	44.6	11.1	767.0	424.1	39.4	8.7	848.3	427.6	42.8	9.8
3	854.0	355.1	39.3	12.7	978.9	414.2	44.6	12.7	827.1	424.1	39.4	10.2	916.3	427.6	42.8	11.4
2	792.8	355.1	39.3	11.1	904.4	414.2	44.6	11.0	782.6	424.1	39.4	9.1	866.9	427.6	42.8	10.3
1	631.1	355.1	39.3	7.0	723.8	414.2	44.6	6.9	645.3	424.1	39.4	5.6	696.6	427.6	42.8	6.3
0	562.8	355.1	39.3	5.3	646.0	414.2	44.6	5.2	590.0	424.1	39.4	4.2	629.3	427.6	42.8	4.7
	Average Light Response			**8.4**	**Average Light Response**			**8.3**	**Average Light Response**			**6.7**	**Average Light Response**			**7.4**
	Overall Average Light Response = 7.758															
	% Deviation from Mean			**8.49%**	**% Deviation from Mean**			**7.32%**	**% Deviation from Mean**			**- 13.20%**	**% Deviation from Mean**			**- 2.60%**

Table 5.1: Light distribution uniformity calculation: The red cells represent points rejected either due to saturation (Delay 6) or due to insufficient or no Light Response (Delays 13, 12 and 11).

The same measurement and calculation were repeated several times and the average light distribution uniformity was calculated. Table 5.2 shows the overall results. The level of uniformity is fair as it ranges from ~ -11% to 8%. In addition, the relatively low values of standard deviation reveal very good consistency. Better uniformity, however, is required.

Measurement	% Deviation of the Light Distribution Uniformity from Mean			
	P49	P51	P53	P56
1	8.49%	7.32%	-13.20%	-2.60 %
2	7.77%	5.57%	-12.31%	-1.04%
3	7.13%	2.03%	-8.27%	-0.89%
Average	**7.80%**	**4.97%**	**-11.26%**	**-1.51%**
Standard Deviation	**0.55%**	**2.20%**	**2.15%**	**0.77%**

Table 5.2: Summary of light distribution uniformity using the LG channel (100-micron-pixel SiPMs).

5.1.2. High Gain Channel

Since the HG channel is expected to have more peaks, which would improve the gain calculation, it was worthwhile calculating the light distribution uniformity with the HG channel. However, since the HG channel leads to early saturation of the SiPMs, many of the LED Delays could not be used for this purpose. In order to overcome the issue of saturation, SiPMs bias voltages were lowered to the lowest possible bias voltages at which photoelectron peaks were still observed. This greatly reduced the issue of saturation and enabled the use of most of the LED Delays. The same measurement and calculation method used for the LG channel was used here. Table 5.3 summarizes the results.

Measurement	% Deviation of the Light Distribution Uniformity from Mean			
	P49	P51	P53	P56
1	9.19%	5.49%	-7.65%	-7.03%
2	8.97%	5.96%	-7.57%	-7.37%
3	5.84%	-5.03%	0.02%	-0.83%
Average	**8.00%**	**2.14%**	**-5.06%**	**-5.08%**
Standard Deviation	**1.53%**	**5.07%**	**3.59%**	**3.01%**

Table 5.3: Summary of light distribution uniformity using the HG channel (100-micron-pixel SiPMs).

In terms of the average percent deviation of the light distribution uniformity from the mean, the HG and the LG channels are consistent. However, the LG channel reveals more coherent results as manifested by the lower values of the standard deviation. This is a plausible result because the much higher gain leads to a higher sensitivity, which causes higher uncertainty due to fluctuations in temperature and the amount of light emitted by the LED, in addition to statistical uncertainty.

5.2. Light Distribution Uniformity Using 50-micron-pixel SiPMs

Similar measurements were performed using 50-micron-pixel SiPMs instead of 100-micron-pixel SiPMs. 50-micron-pixel SiPMs are less sensitive than their 100-micron-pixel counterparts with lower responses, thereby helping minimize the issue of saturation. The SiPMs were optimally biased and all other parameters were kept fixed. However, only the HG channel was used, as the LG channel does not provide any

response with discernible photoelectron peaks. Table 5.4 summarizes the results weighted by the number of hits in each run.

The limited number of peaks observed with a 17 ns pulse leads to high uncertainty in calculating the light distribution uniformity. Therefore, in order to increase the number of peaks and yet obviate saturation; the light pulse was manipulated. It was found out that a pulse 19 ns in width and 2.5 V in amplitude filtered through a white filter would yield the desired results. The rest of the parameters were identical to the previous measurements. Table 5.5 summarizes the results.

As the cased of the 100-micron-pixel SiPMs, there is no significant difference in the average deviations of the light distribution uniformity between the HG and the LG channels; however, the LG channel provides the lower values of the standard deviation.

Run	Number of Hits Per Run	P49	P51	P53	P6
1	1000	- 12.86%	13.71%	14.10%	- 14.95%
2	1000	- 4.50%	3.00%	13.65%	- 12.15%
3	1000	- 8.38%	7.28%	19.25%	- 18.16%
4	15000	-11.90%	6.69%	21.39%	- 16.18%
Average (% Deviation X Number of Hits) / Total Hits		**- 11.34%**	**6.91%**	**20.44%**	**- 16.00%**
Standard Deviation		**3.80%**	**4.45%**	**3.83%**	**2.52%**

Table 5.4: Summary of light distribution uniformity of a 17 ns pulse: HG channel (50-micron-pixel SiPMs).

Measurement	P49	P51	P53	P6
1	- 8.56%	3.83%	17.21%	- 12.48%
2	- 7.83%	3.70%	17.29%	- 13.16%
3	- 7.82%	4.56%	16.40%	- 13.14%
4	- 7.56%	5.65%	15.49%	- 13.57%
Average	**- 7.94%**	**4.43%**	**16.60%**	**- 13.09%**
Standard Deviation	**0.37%**	**0.77%**	**0.73%**	**0.39%**

Table 5.4: Summary of light distribution uniformity of a 19 ns filtered pulse: the HG channel (50-micron-pixel SiPMs).

5.3. Light Distribution Uniformity Summary

Table 5.5 summarizes the light distribution uniformity calculated with two different parameters sets. The 100-micron-pixel SiPMs were investigated with one electronics board and the 50-micron-pixels SiPMs with a second, different electronics board. As the table indicates the response with a single board is consistent between parameter sets. The two boards are expected to have differences especially regarding positioning of the SiPMs, LEDs and scintillator mounting holes. Such discrepancies could yield significant differences in the light distribution uniformity.

SiPM Pixels	Relevant Parameter	P49		P51		P53		P56	
		Mean	SD	Mean	SD	Mean	SD	Mean	SD
100	17ns Pulse Width - LG	7.80%	0.55%	4.97%	2.20%	-11.26%	2.15%	-1.51%	0.77%
	17ns Pulse Width - HG	8.00%	1.53%	2.14%	5.07%	-5.06%	3.59%	-5.08%	3.01%
50	17ns Pulse Width - HG	- 11.34%	3.80%	6.91%	4.45%	20.44%	3.83%	- 16.00%	2.52%
	19ns Pulse Width – HG – Filtered Pulse	- 7.94%	0.37%	4.43%	0.77%	16.60%	0.73%	- 13.09%	0.39%

Table 5.5: Summary of light distribution uniformity of different parameters.

CHAPTER SIX

LIGHT UNIFORMITY SENSITIVITY ANALYSIS

The light distribution uniformity analysis showed high sensitivity to small shifts in the position of the scintillator tiles relative to the LED and SiPMs. For instance, there is a significant difference in the uniformity between one position of the scintillator and another shifted by about 1 mm. Therefore, sensitivity analysis is needed to determine how the scintillator's position affects the overall light distribution uniformity, and to specify manufacturing tolerances for the IRL.

6.1. Jig and its Components

In order to study the sensitivity of the light distribution uniformity to the position of the scintillator or equivalently the position of the LEDs, a jig was manufactured by NIU's Physics Department Machine Shop. This enabled measurable translation of the scintillator relative to the circuit board with the LEDs and sensors. Figure 6.1 shows the jig and its main components.

The jig is made of a rigid base, across which a hinged metallic bridge is mounted. The cross-bridge is secured to the base by means of a screw and can be opened to mount the scintillator. Screwed to the cross-bridge is the head, which holds the moving part of the jig. The moving part of the head includes the mounting platform on which the scintillator is mounted, and two perpendicularly positioned micrometers that move the platform and the scintillator in the X and Y directions by pushing against two anvils attached to the head. The micrometers have inch scales with an accuracy of ± 0.0005 in.

The board is placed on the base and screwed to it through the screw holes. The scintillator is mounted on the platform and the cross-bridge is closed and screwed to the base. The vertical tolerances of the combined jig, IRL board, and scintillator are such that the scintillator is just flush with the SiPMs and LED.

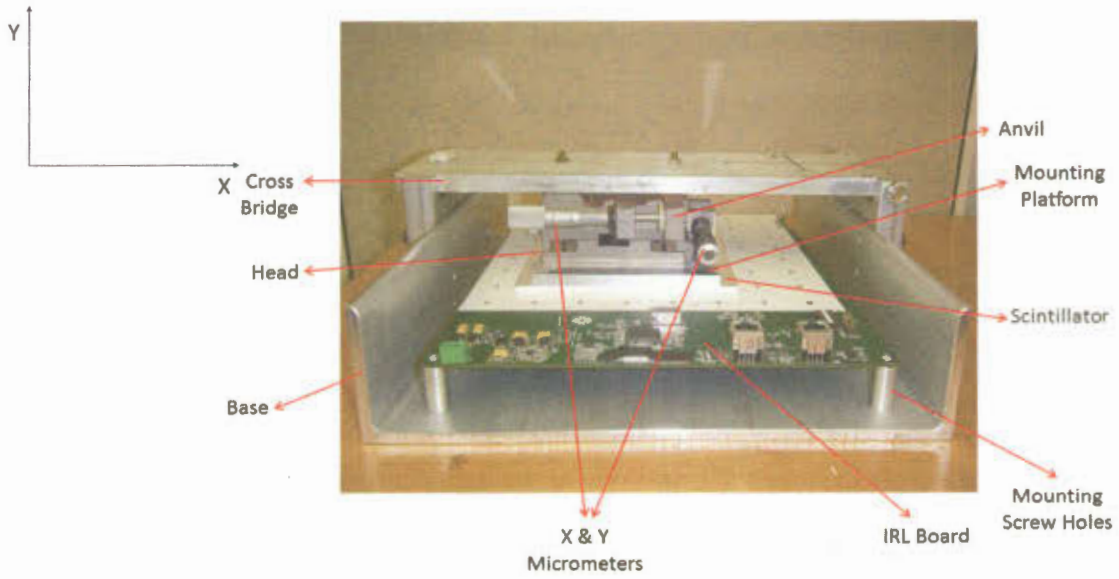

Figure 6.1: Jig and its main components.

6.2. Fitting Photoelectron Peaks

In order to reduce the sources of uncertainty, response histograms were fit with an algorithm developed in Root in order to calculate the response parameters, such as mean, RMS, gain and so forth. Figure 6.2 shows a sample histogram fit with this algorithm. This fit was primarily used to calculate the SiPMs gain values accurately in order to calculate the light distribution uniformity. However, the autofit does not differ from the manual gain determination used for earlier results by more than 2%.

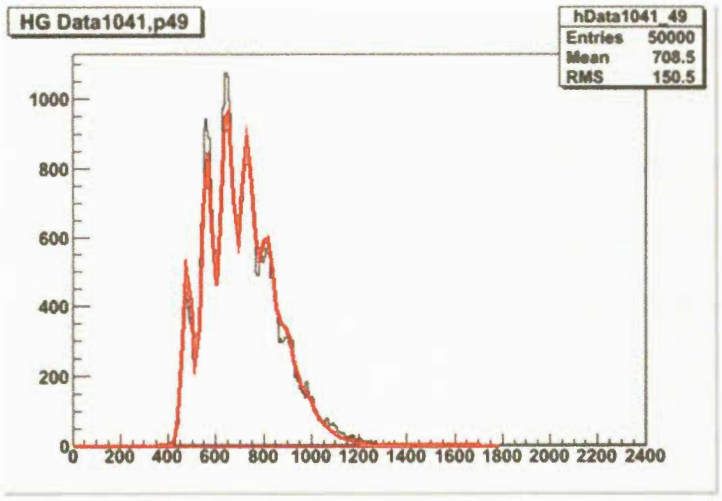

Figure 6.2: Fitting photoelectron peaks.

6.3. X and Y Dependence

In order to perform a sensitivity analysis, the original position of the scintillator when directly coupled to the IRL board was taken as the origin, and scans along the X and Y axes with steps of 0.01 in. were made. At each point, the light distribution uniformity was calculated. Figure 6.3 shows how scans were made.

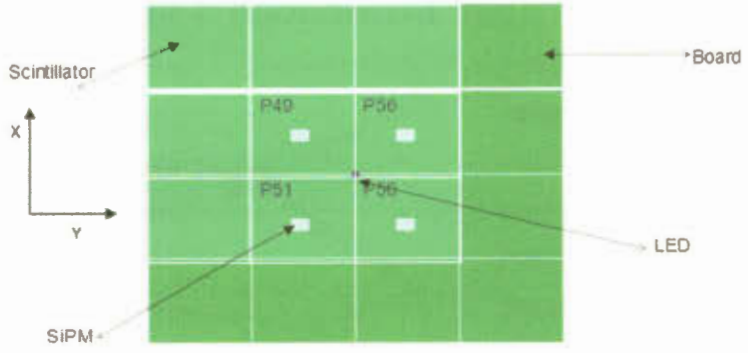

Figure 6.3: Scanning along the X and Y axes: The scintillator (indicated with the transparent white grid) could be moved relative to the circuit board (green).

The light distribution uniformity was calculated as a function of the (X,Y) coordinate in increments of 0.01 inches (0.254 mm). These measurements reveal how sensitive the uniformity is to small shifts in position, and second, they help pinpoint the (X,Y) location with the best uniformity. Figures 6.4 and 6.5 show the dependence of the light distribution uniformity on the X and Y coordinates, respectively.

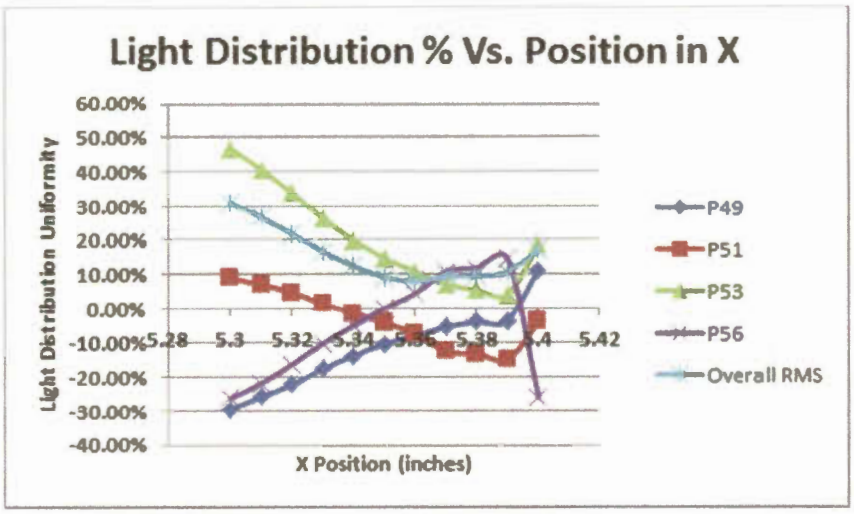

Figure 6.4: Light distribution uniformity as a function of position in X.

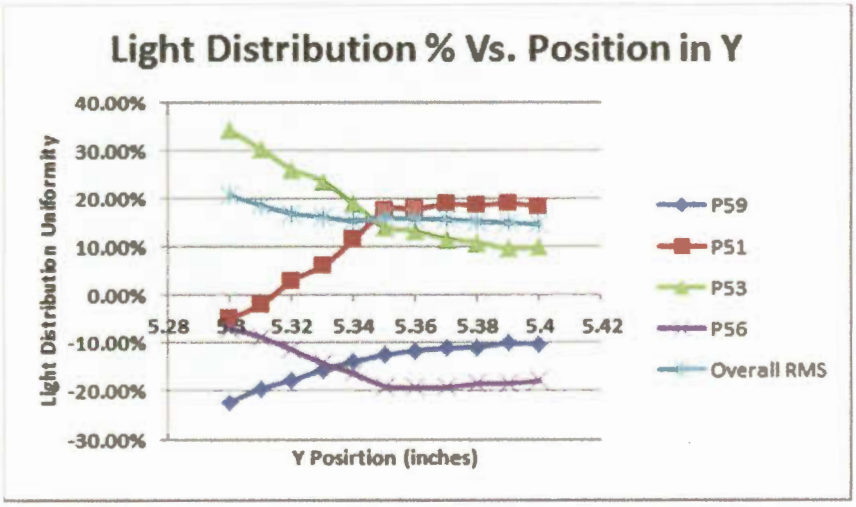

Figure 6.5: Light distribution uniformity as a function of position in Y.

The following points can be inferred from the two plots:

1. The change in the uniformity versus translation is different for the X and Y directions, and for each case, the change in the uniformity is not constant. This is plausible because the largest changes in the light distribution uniformity correspond to positions where the inter-tile paint separating four adjacent tiles is nearly coincident with the LED. At such a point, small shifts in position can drastically alter the amount of light received by each SiPM, since small translations shift a significant amount of light from one SiPM to another.
2. At the starting point, the percent deviations in the light distribution uniformity for each SiPM, as demonstrated by the overall RMS, are significant. As the scintillator is translated in one direction, the deviations decrease to a certain level before increasing again. The two points of the X and Y plots representing these local minima correspond to the location where the inter-tile paint separating between four adjacent tiles is closest to the center of the LED. This location represents the point where the best uniformity is expected.
3. The X plot reveals that in the vicinity of the local minimum, the sensitivity of the light distribution uniformity to position shifts is maximal. On the other hand, the uniformity is relatively insensitive to translations in the Y direction. This is due to mismatch between the center of the LED and center of the inter-tile paint, which causes the two axes to show different behaviors.

6.4. Best Light Distribution Uniformity

The local minima described above were taken as the coordinates of the new origin in order to calculate the light distribution uniformity. It was found that uniformity within ± 5% can be achieved for all SiPMs. Such uniformity is better that originally anticipated. The uniformity was recalculated several times in order to ensure reproducibility and stability. Table 6.1 summarizes the results.

Coordinate (in.)		**% Deviation of Light Distribution Uniformity from Mean**				**Range**	**RMS**
X	**Y**						
5.36	**5.35**	0.43%	4.49%	- 0.32%	- 4.60%	9.09%	3.22%
5.36	**5.35**	1.35%	3.17%	- 0.12%	- 4.40%	7.57%	2.79%
5.36	**5.35**	1.62%	4.05%	- 1.02%	- 4.65%	8.70%	3.23%
5.36	**5.35**	1.83%	4.50%	- 1.34%	- 4.99%	9.48 %	3.54%
5.36	**5.35**	1.29%	4.16%	- 0.81%	- 4.64%	8.81%	3.21%
5.36	**5.35**	0.77%	4.89%	- 2.07%	- 3.59%	8.48%	3.23%
5.36	**5.35**	0.80%	4.58%	- 1.60%	- 3.78%	8.36%	3.10%
5.36	**5.35**	0.67%	4.59%	- 1.30%	- 3.97%	8.56%	3.12%
5.36	**5.35**	0.51%	4.16%	0.35%	- 5.02%	9.18%	3.27%
5.36	**5.35**	0.18%	4.79%	- 0.48%	- 4.49%	9.28%	3.29%
Average		**0.95%**	**4.34%**	**- 0.87%**	**- 4.41%**	**8.75%**	**3.20%**
RMS		**0.34%**	**1.38%**	**0.35%**	**1.40%**	**2.77%**	**1.01%**

Table 6.1: Best light distribution uniformity achieved.

Table 6.1 also shows that the light distribution uniformity for the SiPMs is stable. The RMS of the four SiPMs is less than 3%. Again, this result exceeds what was

originally anticipated given the manual installation and manufacturing of the IRL board and the jig.

Figure 6.6 shows the stability of the light distribution uniformity for each trial of the four SiPMs individually. Figure 6.7 shows the stability of the four SiPMs. The RMS of the four SiPM response values has been calculated and plotted in Fig. 6.7 for each trail. The straight line is the average RMS for all ten trials.

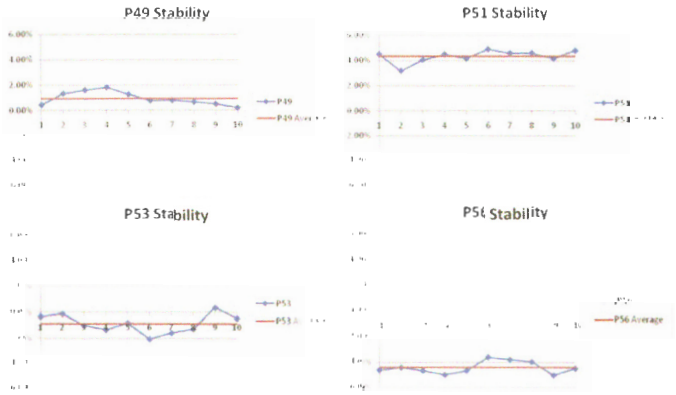

Figure 6.6: Individual stability of the light distribution uniformity of the four SiPMs as a function of trial number.

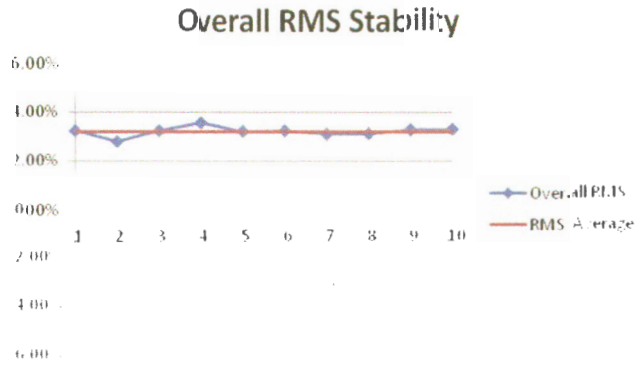

Figure 6.7: Overall stability of the light distribution uniformity of the four SiPMs as a function of trial number.

6.5. Position Tolerance

Position tolerance refers to the maximum displacement of the scintillator from the origin that can be tolerated while keeping the deviations in the light distribution uniformity within acceptable levels. Setting the maximum permissible deviation to 10%; the position tolerance can be estimated from Figures 6.4 and 6.5 above. However, this runs into a difficulty as the changes in the uniformity are dissimilar in the X and in the Y directions.

To overcome this difficulty, the more sensitive axis (i.e. the X axis) is used for estimation, and the tolerance is calculated for the point corresponding to the best uniformity. If the overall uniformity (i.e. the overall RMS of the percent deviation of the uniformity) is taken as measure, then the maximum position tolerance would be $\pm$ 0.01 inches. This is rather a conservative estimate, since it includes all SiPMs collectively. In addition, the results obtained from the jig analysis contain an unavoidable source of uncertainty as the jig's axes are rotated with the respect to board's axes by ~ 0.5°. This tilt is expected to have contributed significantly to the non-uniformity of light distribution.

A better method would be to estimate the tolerance of each SiPM separately and relative to its own minimum deviation, and then take the lowest tolerance as the overall tolerance. Table 6.2 presents the position tolerance of each SiPM.

SiPM	P49	P51	P53	P56
Tolerance (in.)	± 0.03	± 0.02	± 0.02	± 0.02

Table 6.2: Position Tolerance of the four SiPMs.

As Table 6.2 reveals, the position tolerance using the 10% deviation metric for 50-micron-pixel SiPMs is estimated to be 0.02 inches (~ 0.051 cm). However, eliminating the major source of uncertainty represented by the misalignment of the jig is expected to improve the tolerance.

CHAPTER SEVEN

A BRIEF DISCUSSION OF TEMPERATURE EFFECT

SiPMs are sensitive to temperature. In particular, their gain is expected to drop as temperature increases. This dependence can pose difficulties in calibration, since data taking was not done in a temperature-controlled environment. This chapter presents a brief discussion of temperature effects on both gain and light distribution uniformity. The analysis here does not represent an exhaustive study of temperature effects. However, it helps understand the effects of temperature to be taken into consideration for calibration purposes.

7.1. Effect on Gain

Data runs were taken at different temperatures, and the gain values were calculated for each run. To ensure accuracy, only data runs where temperature was fixed throughout the entire run duration were kept, and other runs during which temperature changed were discarded. As expected, the gain values drop as temperature increases. This drop can reach ~ 7% / $^{\circ}$C as table 7.1 shows. Figure 7.1 shows gain as a function of temperature for four 50-micron-pixel SiPMs.

Temp. (◦ C)	Gain			
	P49	P51	P53	P56
26.8	81.13	82.80	83.08	84.53
26.7	80.97	81.63	83.85	85.80
26.6	81.90	83.77	84.50	86.00
26.5	82.47	83.93	84.05	86.70
26.4	83.27	85.45	86.23	87.37
26.3	83.30	84.87	85.23	87.30
26.2	83.53	84.87	85.43	88.63
% Gain Change / ◦ C	- 5.34%	- 4.99%	- 5.18%	- 6.55%

Table 7.1: SiPMs gain percent change as a function of temperature.

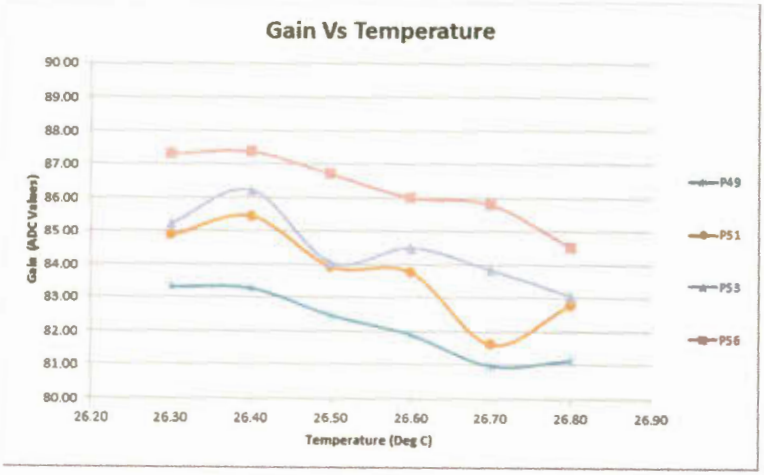

Figure 7.1: SiPMs gain as a function of temperature.

7.2. Effect on Light Distribution Uniformity

In spite of the fact that temperature affects gain, it is not expected to affect the light distribution uniformity, since uniformity only depends on the geometric arrangement of

scintillator, the LED and the SiPMs. Indeed, there is no evidence that temperature effects light distribution uniformity as Table 7.2 and Figure 7.2 demonstrate.

Temp. (◦ C)	Light Distribution Uniformity			
	P49	P51	P53	P56
26.8	- 8.56%	3.83%	17.21%	- 12.48%
26.7	- 6.98%	2.27%	16.59%	- 11.88%
26.6	- 7.83%	3.70%	17.29%	- 13.16%
26.5	- 7.82%	4.56%	16.40%	- 13.14%
26.4	- 7.56%	5.65%	15.49%	- 13.57%
26.3	- 8.69%	4.26%	16.29%	- 11.86%
Mean	**- 7.91%**	**4.04%**	**16.55%**	**- 12.68%**
Standard Deviation	**0.58%**	**1.02%**	**0.61%**	**0.65%**

Table 7.2: Temperature and light distribution uniformity.

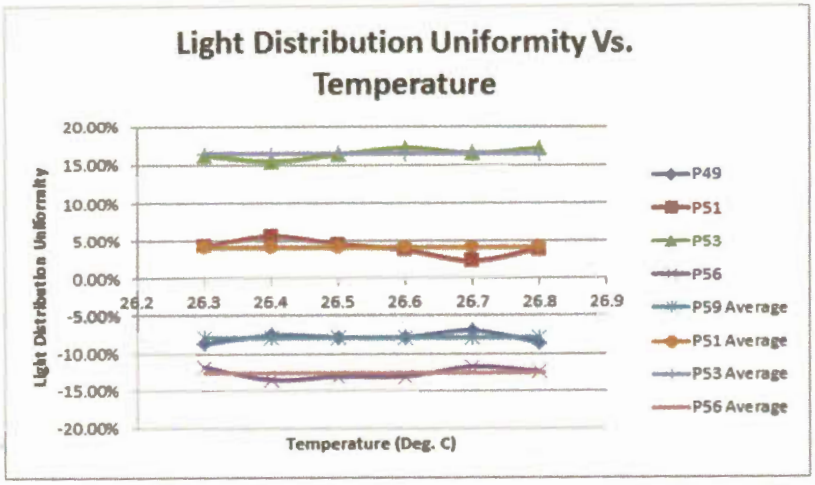

Figure 7.2: SiPMs light distribution uniformity as a function of temperature.

CHAPTER EIGHT

DESIGN ISSUES AND PROPOSED ENHANCEMENTS

8.1. Design Issues

The IRL board used for data taking and analysis is a first version. It was designed by NICADD and manufactured by the Department of Electrical Engineering at Fermilab. Electronics such as SiPMs and LEDs were installed manually. Therefore, this pilot board experienced several issues and limitations, most critical of which are the following:

1. **Installation of the SiPMs and LEDs and Positioning of the Scintillator**

   The most critical issue is the positioning of the SiPMs, LEDs and the scintillator. As presented in Chapter 6, the light distribution uniformity is sensitive to small deviations and/or rotations of the SiPMs, LEDs and scintillating tiles from their presupposed positions.

   Since the SiPMs and the LEDs were manually installed, and since the scintillator's mounting holes were manually drilled, deviations from the original design did occur. The light distribution uniformity is limited by these deviations in position and alignment.

2. **Saturation**

   The second most serious issue of the IRL is response saturation. Saturation is related to the number of bits the ADC has and the level of amplification its amplifier circuit provides. Saturation limits the

functionality of the IRL. Saturation occurs at ADC = 2047 which corresponds to 2^{11} (since the ADC range includes 0). This means that either the ADC dynamic range is insufficient, or that the amplification provided by the amplification circuit is higher than necessary, or both.

3. Controlling the Amount of Light

Another major issue the IRL and the front-end electronics have is the difficulty and inflexibility of controlling the amount of light emitted by the calibration LEDs. Since the electric pulse delivered to the LED is connected to the crystal oscillator, it can only be manipulated through reprogramming the firmware (the software hosted by the CRIM and the CROC) and can only yield a discrete set of pulses that have fixed widths and amplitudes. Therefore, the amount of light generated by the LED cannot be flexibly manipulated to enable more complete calibration.

The inflexibility in controlling the amount of light is also related to the slowness of the comparator. The comparator is an electronic chip that provides the output that activates the LEDs. When the gate opens; the comparator is supposed to reach its maximum value quickly and before the gate closes. The fact that minor manipulation of the pulse width and amplitude can result in either saturation (too much light) or no light emitted at all reveals the fact that the comparator's rise time is long, such that its output does not reach a certain value enough to activate the LED. Figure 8.1 illustrates the situation.

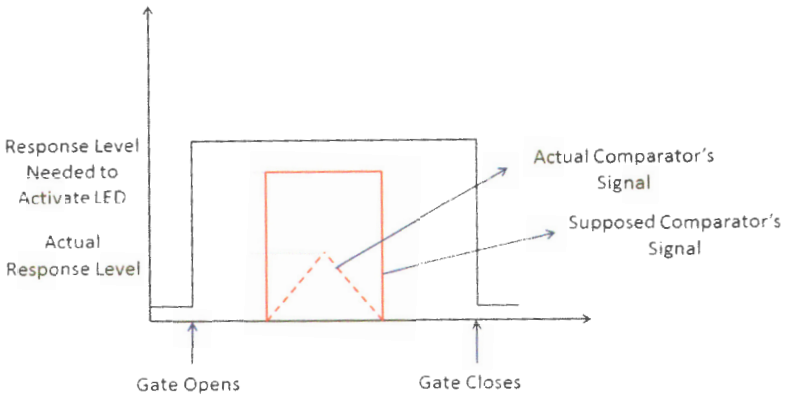

Figure 8.1: Comparator's actual response.

4. Ostensible Gain Dependence on LED Delay

As illustrated in Section 4.2.5, the time constant of the integrator is long (30 ns), which inhibits its output from reaching a maximum value at some LED Delay. This reduces the output and makes their gain appear to depend on the LED Delay. This ostensible dependence can lead to errors in calculating the light distribution uniformity should the wrong LED Delay be taken for calculation.

5. LEDs Time Constant (τ)

The time constant of the calibration LEDs is quite long in comparison with the other time scales of the IRL operation, such as the LED Delay and the Gate Length. The long time constant suggests that either the LEDs, the comparator that delivers the electric pulse to the LEDs, or both are slower than the measurement parameters.

The large time constant leads to slow exponential rise and decay of the light pulse emitted by the LED. In particular, the slow exponential decay leads to a long tail of the light pulse that extends beyond the end of the gate. This causes part of the light pulse to be clipped, which reduces the SiPMs response and affects the clarity of photoelectron peaks.

6. **Temperature variation**

As presented in Chapter 7, SiPMs are sensitive to temperature and their gain decreases as temperature increases; however, in terms of uniformity this issue is fairly benign since there is no evidence that temperature variation affects light distribution uniformity.

8.2. Design Enhancements

Several enhancements can be made to the IRL in order to overcome the limitations discussed above. The major design enhancements include the following:

1. **Careful Installation and Positioning**

It is important to carefully install SiPMs and LEDs on the IRL board such that the deviations from design locations are minimal. This includes perfect coincidence of the SiPMs centers with the centers of installation location on the board, and maintaining the sensitive surfaces perfectly horizontal. In addition, the sensitive surface of the SiPM and the light-reflecting surface on the IRL board should be at the same horizontal level

with no gap between them in order to make the whole surface just flush with the scintillator.

The scintillator should be perfectly coupled to the IRL board such that the center of the inter-tile paint separating four adjacent tiles coincides with the center of the calibration LED, and such that each dimple center coincides with the center of the SiPM installed beneath it. The deviations from the designed position should not exceed $\pm$ 0.02 inches (0.051mm) in order to maintain the light distribution uniformity within 10%.

Careful positioning is expected to yield even better light distribution uniformity, improve calibration and help achieve more accurate measurements.

2. Reducing Time Constant (τ)

Since the time constant of the LED is very long compared to the time scale of other parameters, much of the tail of the light pulse is clipped and not integrated by the gate. Therefore, the LED time constant needs to be reduced, such that only a negligible fraction of the pulse is clipped. Although clipping a portion of light does not affect gain and does not affect the results pertaining to this experiment, it is worth discussing.

Since the amount of light emitted by the LED is proportional to the electric pulse delivered to it, voltage can be taken as a measure of the amount of light. If σ is the fraction of light clipped by the gate, then the time constant of the LED can be calculated as follows:

$$\tau = \frac{T}{\ln(\sigma)}$$

Where T is the time interval separation between the pulse maximum and the gate closing, calculated by subtracting the LED Delay value at which the SiPMs response reaches a maximum from the total Gate Length. For example, for a 13 tick Gate Length, if the amount of light to be clipped is not to exceed 0.1%, and 50-micron-pixel SiPMs are used (where they peak at 3 ticks delay), then T = 10 ticks, and the time constant should be ~ 1.5 tick or 13.6 ns.

Clipping 0.1% of the light has negligible effect on the response, since statistical variations become dominant at this level. Therefore the time constant of the LED should be close to 13.6 ns, The LED comparator should be selected to achieve the desired time constant.

3. Electronics Selection

The electronics used in making the IRL, particularly the ADC, have an 11-bit saturation issue. Although the ADC provides 12 bits, one bit is used in order to achieve synchronization with the FPGA. This leads to undesired early saturation in addition to other limitations. In order to minimize the issue of saturation; more capable electronics should be selected. The selection of the electronics depends on the SiPMs response value at which no saturation is to occur, which in turn is determined by the working environment in which the IRL is intended to operate.

In general, 14 - 18 bit ADCs are available, which means that the available ADC range can be increased from the current 2047 to 8192 ADC counts (for a 14-bit ADC, i.e. 2^{13}, since one bit is to be used to achieve synchronization with the FPGA) or 131072 ADC counts (for an 18-bit ADC, i.e. 2^{17}). Judging by the mean values obtained throughout this study, a 14-bit ADC should be enough for both the 50-micron-pixel and the 100-micron-pixel SiPMs.

Another important issue is the comparator. A comparator with a short rise time is needed, such that its response can reach a level high enough to activate the LED before the gate closes, as illustrated in Figure 8.1.

Another important drawback that needs to be overcome is the slowness of the integrator. The integrator has a time constant of 30 ns, which is long compared with the other parameters. Therefore, a comparator with a shorter time constant is needed.

4. Light Amount Control

Introducing a mechanism to control the amount of LED light would greatly enhance the flexibility of calibration. However, since the electric pulse is controlled by the front-end electronics (namely the CRIM and the CROC), any mechanism requires a complete reprogramming of the firmware.

An alternative method lies in the IRL hardware. It is possible to install variable resistors in the LED supporting circuits to control the amount of current passing through the LEDs. The drawback of this alternative is that

calibration of the resistors is needed. If this method is to be applied, then the range of the resistance should be from zero up to an arbitrarily large value that would practically extinguish all light emitted. This way a precise value that optimizes the amount of light can be determined.

5. SiPMs Selection

Hamamatsu SiPMs represent an excellent choice that supports high sensitivity. However, either 50-micron-pixel or 100-pxel SiPMs should be used with the IRL, as 25-micron-pixel SiPMs have very limited sensitivity, and their response does not show any photoelectron peaks.

CHAPTER NINE

CONCLUSION

The concept of direct coupling represented by the IRL board is a promising one. In spite of the current design issues and limitations; the IRL demonstrates both functionality and effectiveness. Light generated through scintillation can be conveyed to SiPMs directly, thereby eliminating the need for fiber optics. In addition, the high sensitivity of SiPMs and the very good light distribution uniformity (within $\pm$ 5%), make the IRL an excellent candidate for precision calorimetry.

Careful installation of SiPMs and LEDs and accurate coupling of the scintillator are vital to attain a uniform light distribution. SiPMs are highly sensitive to small increments in the amount of light. Therefore, in order to maintain light distribution uniformity within 10%, the scintillator should not deviate by more than $\pm$ 0.02 inches from its nominal position.

Improvements are to be implemented to the IRL and an enhanced version is to be manufactured in the near future. This version, after being briefly characterized to ensure that the issues and limitations of the original board have been surmounted, will be used for data collection in a test beam at Fermilab.

REFERENCES

[1] http://lhc.web.cern.ch/lhc/

[2] K. Francis, Evaluating Small Scintillating Cells for Digital Hadron Calorimeters: Master Thesis, Northern Illinois University, p1-2 (2004)

[3] http://www.linearcollider.org/about/Why-do-we-need-the-ILC/The-science

[4] Detectors for a Future Lepton Collider Lecture 3: Calorimetry, http://www.hep.phy.cam.ac.uk/~thomson/talks/CERN_Academic_Training_Lecture_III_Final.pdf (2010)

[5] C. Adolff et al., Study of the Interactions of Pions in the CALICE Silicon-Tungsten Calorimeter Prototype, p1 (2010)

[6] The International Linear Collider Passport, http://www.linearcollider.org/pdf/ilc_gateway_report.pdf

[7] G. Blazey et al., Directly Coupled Tiles as Elements of Scintillator Calorimeter with MPPC Readout, Nuclear Instruments and Methods in Physics Research A (2009)

[8] MPPC, Multi-Pixel Photon Counter: Hamamatsu Product Catalogue, http://sales.hamamatsu.com/assets/applications/SSD/mppc_kapd0002e08.pdf

[9] S. Tavernier experimental techniques in nuclear and particle physics, Springer, p167 (2010)

[10] B. Baldin, VME Data Acquisition Modules for MINERvA Experiment, Fermi National Accelerator Laboratory